Proceedings of the Tenth Pacific Conference on Earthquake Engineering
Building an Earthquake-Resilient Pacific
6-8 November 2015, Sydney, Australia

Seismic response analysis of a coupled (curved railway) bridge – train system under frequent earthquakes

Qing Zeng & Elias G. Dimitrakopoulos

Department of Civil and Environmental Engineering, The Hong Kong University of Science and Technology, Clear Water Bay, Kowloon, Hong Kong.

ABSTRACT: This paper investigates the seismic response of a coupled vehicle-bridge system. The bridge is a five-span, horizontally curved, continuous railway bridge. The bridge is modeled by finite elements while the train vehicles are represented by multibody assemblies, in all three dimensions (3D). The study verifies that the conventional seismic response analysis method, which considers the vehicles merely as additional mass, yields a conservative estimation of the response of the bridge. Specifically, the results verify the favorable damping effect the running vehicles have on the vibration of the deck. By contrast, the analysis underlines the adverse effect the vibration of the bridge has on the seismic response of the running vehicles. The paper shows that even frequent earthquakes, of moderate intensity, can threaten the safety of vehicles running on seismically excited bridges, in accordance with recorded accidents.

1 INTRODUCTION

The rapid increase of railway networks, worldwide and especially in China, brings about an enhanced role for bridges in contemporary railway infrastructure. For instance, 1059 km of the 1318 km long (80.5%) Beijing-Shanghai high-speed railway (HSR) line in China are on bridges (Xia et al. 2012). Similarly, the ratio of the bridge length to the total length of the Beijing-Tianjin line in China, reaches 86.6% (Xia et al. 2012). In addition, the longest bridge system in the world (Xia et al. 2012) is the 164 km Danyang-Kunshan Grand Bridge of the Beijing-Shanghai HSR line, with over 4000 spans.

The increasing number and length of railway bridges raise the probability of trains encountering an earthquake when running over a bridge accordingly. Two alarming accidents were already reported in the past ten years. On 23 October 2004, a Shinkansen high-speed train derailed during the Niigata Chetsu Earthquake, when running on viaducts at a speed of 200 km/h, breaking the 48-year safety record of the Shinkansen (Xia et al. 2006). On 04 March 2010, a Taiwan HSR train derailed during the 6.4 magnitude Jiasian Earthquake with a speed of 298 km/h, and it fully stopped after running a distance of 3.62 km (Ju 2012). The recent developments in railway transportation, and the reported accidents, bring forward the great importance of the seismic response of coupled vehicle-bridge systems problem, which is currently attracting the attention of researchers all around the world. For instance, Kim et al. (2007) studied the seismic response of steel monorail bridges under moderate earthquakes. They concluded that the conventional approach suggested by most seismic codes worldwide (e.g. EC8 1998) which treats the train vehicles merely as additional mass, overestimates the seismic response of bridges. Xia et al. (2006) and Du et al. (2012) examined the dynamic interaction of bridge-train systems under non-uniform seismic ground excitations, and argued that the consideration of the seismic wave propagation effect is important to the running safety of vehicles during earthquakes.

Despite the abundance of studies on the seismic response of bridges in the absence of the vehicle dynamics (see for instance Kappos et al. 2012 and references therein), or on the dynamic vehicle-bridge interaction (VBI) without earthquakes (e.g. Dimitrakopoulos & Zeng 2015 and references therein), studies on the seismic response of the coupled bridge-vehicle dynamics are limited. Given the potentially devastating consequences of future seismic accidents, this research shifts the focus of seismic analysis from solely the bridge structure, to the effect of the seismic response of the bridge to the response of the vehicle. The scope of this paper is to present a versatile numerical scheme to simulate the seismic response of the coupled vehicle-bridge system, in all three spatial dimensions (3D's).

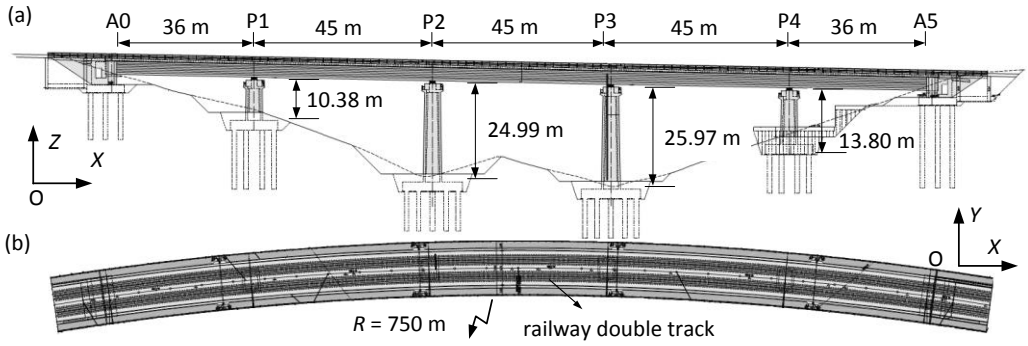

Figure 1. The examined curved railway bridge: (a) elevation, (b) plan view.

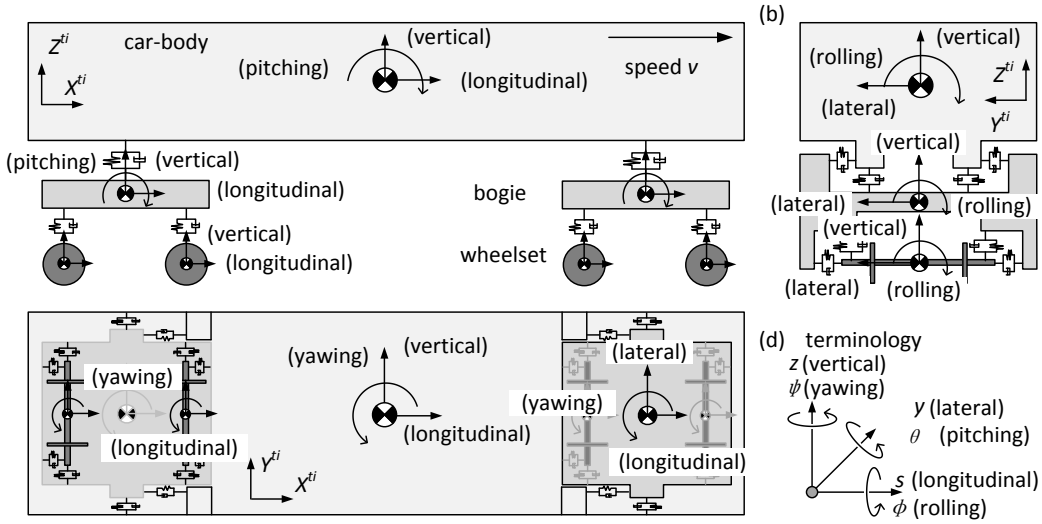

Figure 2. The vehicle model (a) elevation view, (b) back view, (c) top view, and (d) terminology.

2 PROPOSED MODEL

2.1 Bridge modelling

Figure 1 plots the bridge examined in the study, which is a horizontally curved continuous concrete double-line railway bridge in a seismic prone area. The radius of curvature is 750 m and the length of the bridge is 207 m (Figure 1). The complete geometrical model of the bridge is built with finite elements. The equation of motion (EOM) of the bridge system takes the form:

$$\mathbf{M}^B\ddot{\mathbf{u}}^B + \mathbf{C}^B\dot{\mathbf{u}}^B + \mathbf{K}^B\mathbf{u}^B - \mathbf{W}_N^B\boldsymbol{\lambda}_N - \mathbf{W}_T^B\boldsymbol{\lambda}_T = \mathbf{F}^B \tag{1}$$

where, the superscript $(\,)^B$ denotes the bridge system and throughout this paper, the upper-dot indicates the differentiation with respect to time. $\mathbf{u}^B$ is the displacement vector of the bridge, $\mathbf{F}^B$ is the vector of the loads of the bridge, containing the seismic loadings when considered:

$$\mathbf{F}^B = -{}_I\ddot{\mathbf{r}}_{OO^G}\boldsymbol{\delta}^B\mathbf{M}^B \tag{2}$$

in which ${}_I\ddot{\mathbf{r}}_{OO^G}$ is the ground acceleration at the base of the bridge, and $\boldsymbol{\delta}^B$ is a unit vector connecting the components of the seismic excitation to the pertinent DOF's of the bridge. $\mathbf{W}_N^B$ and $\mathbf{W}_T^B$ are the pertinent direction matrices, containing the linear shape functions for the axial and torsional degrees of freedom (DOF's) and the cubic (Hermitian) shape functions for the flexural DOF's (Cook 2007), corresponding to the contact forces $\boldsymbol{\lambda}_N$ and $\boldsymbol{\lambda}_T$ (Section 2.3). The effective (reduced) flexural stiffness of the piers and the effective stiffness of the deck due to the cracking of the concrete section during an earthquake is taken as half the uncracked stiffness (EC8 1998). The focus

herein is on frequent, low amplitude earthquake excitations that do not activate the isolation system (e.g. the friction pendulums), or do not force the bridge to behave inelastically/nonlinearly. The study assumes a hypothetical bridge model, considering a monolithic connection between the deck and the piers under moderate earthquakes. For simplicity, the study assumes the piers are fixed at the base.

2.2 **Vehicle modelling**

In this study, each train vehicle is modelled as a multibody assembly. The vehicle consists of one car-body, two bogies and four wheelsets (Figure 2). All components are considered as rigid bodies, neglecting their elastic deformations. The distinct components are connected with springs and dampers, simulating the suspension system. The total DOF's of each vehicle is 38: the car-body and the bogies have 6 DOF's each, and each wheelset holds 5 DOF's (Figure 2).

To describe the motion of the vehicle running along a horizontally curved path, the study employs an additional *moving trajectory system TI*, except from the inertial system I and the body-fixed system *IR*. The motion of the *moving trajectory system* is defined by a time-dependent coordinate, the arc length s^i. The EOM for the vehicle subsystem is:

$$\mathbf{M}^V\ddot{\mathbf{u}}^V + \mathbf{C}^V\dot{\mathbf{u}}^V + \mathbf{K}^V\mathbf{u}^V - \mathbf{W}_N^V\boldsymbol{\lambda}_N - \mathbf{W}_T^V\boldsymbol{\lambda}_T = \mathbf{F}^V \tag{3}$$

where the superscript $(\,)^V$ denotes the vehicle system. The mass matrix $\mathbf{M}^V(t)$ is time-dependent, due to the curvature of the running path,. Considering a specific rigid body component of the vehicle (with a superscript *i*), e.g. a wheelset, its mass submatrix takes the form:

$$\mathbf{M}^i(t) = {}_I\mathbf{L}^i(t)^{\mathrm{T}}\, m^i\, {}_I\mathbf{L}^i(t) + {}_{IR}\mathbf{H}^i(t)^{\mathrm{T}}\, {}_{IR}\mathbf{I}^i_{\theta\theta}\, {}_{IR}\mathbf{H}^i(t) \tag{4}$$

where m^i is the mass of the rigid body i and ${}_{IR}\mathbf{I}^i_{\theta\theta}$ is the inertia tensor about the principal axes. ${}_I\mathbf{L}^i(t)$ and ${}_{IR}\mathbf{H}^i(t)$ are time-varying velocity transformation matrices, pertaining to the translational and the rotational DOF's. The left-subscripts ${}_I(\,)$ and ${}_{IR}(\,)$ denote the reference systems each vector/matrix is referring to. $\mathbf{K}^V$ and $\mathbf{C}^V$ are the stiffness matrix and the damping matrix of the vehicle, given in Antol ń et al. (2013). $\mathbf{W}_N^V$ and $\mathbf{W}_T^V$ are the pertinent contact direction matrices, corresponding to normal and tangential contact forces $\boldsymbol{\lambda}_N$ and $\boldsymbol{\lambda}_T$. $\mathbf{F}^V$ is the vector of external forces:

$$\mathbf{F}^V = \mathbf{F}_g^V + \mathbf{F}_v^V + \mathbf{F}_G^V \tag{5}$$

where $\mathbf{F}_g^V$ is the gravitational force vector; $\mathbf{F}_v^V$ is the inertial force vector, which contains the centrifugal forces and the coriolis forces due to the running curved path. The inertial force vector $\mathbf{F}_v^i$ (due to the curved trajectory) of a single rigid body i is:

$$\mathbf{F}_v^i = -m^i\, {}_I\mathbf{L}^i(t)^{\mathrm{T}}\, {}_I\boldsymbol{\gamma}_R^i - {}_{IR}\mathbf{H}^i(t)^{\mathrm{T}}\left({}_{IR}\mathbf{I}^i_{\theta\theta}\, {}_{IR}\boldsymbol{\gamma}_\alpha^i + {}_{IR}\boldsymbol{\omega}^i \times \left({}_{IR}\mathbf{I}^i_{\theta\theta}\, {}_{IR}\boldsymbol{\omega}^i\right)\right) \tag{6}$$

where ${}_{IR}\boldsymbol{\omega}^i$ is the angular velocity vector of the rigid body. The vectors ${}_I\boldsymbol{\gamma}_R^i$ and ${}_{IR}\boldsymbol{\gamma}_\alpha^i$ are additional quadratic velocity terms, due to the time-differentiation of the absolute translational and absolute angular velocities, respectively (Dimitrakopoulos & Zeng 2015). $\mathbf{F}_G^V$ is the seismic loading on the vehicle system:

$$\mathbf{F}_G^i = -m^i\, {}_I\mathbf{L}^i(t)^{\mathrm{T}}\, {}_I\ddot{\mathbf{r}}_{OO^G} \tag{7}$$

2.3 **Vehicle-bridge interaction**

Based on the EOM's (1) and (3), the EOM of the coupled vehicle-bridge system is:

$$\mathbf{M}^*\ddot{\mathbf{u}} + \mathbf{C}\dot{\mathbf{u}} + \mathbf{K}\mathbf{u} - \mathbf{W}_N\boldsymbol{\lambda}_N - \mathbf{W}_T\boldsymbol{\lambda}_T = \mathbf{F} \tag{8}$$

where the global displacement vector $\mathbf{u}$, the global mass $\mathbf{M}^*$, the stiffness $\mathbf{K}$ and damping $\mathbf{C}$ matrix and the global force vector $\mathbf{F}$ are created by gathering the pertinent matrices of the two individual

subsystems as:

$$\mathbf{u}=\begin{bmatrix}\mathbf{u}^V\\ \mathbf{u}^B\end{bmatrix},\ \mathbf{M}^*=\begin{bmatrix}\mathbf{M}^V & \mathbf{0}\\ \mathbf{0} & \mathbf{M}^B\end{bmatrix},\ \mathbf{C}=\begin{bmatrix}\mathbf{C}^V & \mathbf{0}\\ \mathbf{0} & \mathbf{C}^B\end{bmatrix},\ \mathbf{K}=\begin{bmatrix}\mathbf{K}^V & \mathbf{0}\\ \mathbf{0} & \mathbf{K}^B\end{bmatrix},\ \mathbf{F}\ =\ \begin{bmatrix}\mathbf{F}^V\\ \mathbf{F}^B\end{bmatrix} \tag{9}$$

In the normal direction of contact, the study assumes that the wheel is always in contact with the rail - a "rigid-contact" assumption, which is checked after each analysis. As a kinematic constraint, this assumption assumes that the relative acceleration between the wheel and the rail is zero. In the tangential direction of contact, the rolling contact between the wheel and the rail generates the lateral and the longitudinal creep forces, and the spin moments. To account for the high creepage between the wheel and the rail during earthquakes, the calculation of the creep forces adopts the nonlinear Shen-Hedrick-Euristic creep model (Shen et al. 1983). The EOM for the coupled bridge-vehicle system can take the form (Dimitrakopoulos & Zeng 2015):

$$\mathbf{M}^*(t)\ddot{\mathbf{u}}(t)+\mathbf{C}^*(t)\dot{\mathbf{u}}(t)+\mathbf{K}^*(t)\mathbf{u}(t)=\mathbf{F}^*(t) \tag{10}$$

with:

$$\begin{cases}\mathbf{C}^*(t)=\left[\mathbf{E}-\mathbf{W}_N(t)\mathbf{G}_{NN}^{-1}(t)\mathbf{W}_N{}^{\mathrm{T}}(t)\mathbf{M}^{*-1}(t)\right]\left(\mathbf{C}+\mathbf{C}_\xi(t)\right)+2v\mathbf{W}_N(t)\mathbf{G}_{NN}^{-1}(t)\mathbf{W}_N''{}^{\mathrm{T}}(t)\\ \mathbf{K}^*(t)=\left[\mathbf{E}-\mathbf{W}_N(t)\mathbf{G}_{NN}^{-1}(t)\mathbf{W}_N{}^{\mathrm{T}}(t)\mathbf{M}^{*-1}(t)\right]\mathbf{K}+v^2\mathbf{W}_N(t)\mathbf{G}_{NN}^{-1}(t)\mathbf{W}_N'{}^{\mathrm{T}}(t)\\ \mathbf{F}^*(t)=\left[\mathbf{E}-\mathbf{W}_N(t)\mathbf{G}_{NN}^{-1}(t)\mathbf{W}_N{}^{\mathrm{T}}(t)\mathbf{M}^{*-1}(t)\right]\left(\mathbf{F}(t)-\mathbf{F}_\xi(t)\right)-v^2\mathbf{W}_N(t)\mathbf{G}_{NN}^{-1}(t)\mathbf{r}_{cN}''\end{cases} \tag{11}$$

where $\mathbf{E}$ is a unit matrix, and v is the velocity of the vehicle. $\mathbf{G}_{NN}=\mathbf{W}_N{}^{\mathrm{T}}\mathbf{M}^*(t)^{-1}\mathbf{W}_N$ and its inverse $\mathbf{G}_{NN}^{-1}$ strands for the mass participates in the normal contact. $\mathbf{C}_\xi$ and $\mathbf{F}_\xi$ are the equivalent damping matrix and force vector due to creep forces. The symbol $(\,)^*$ indicates that the matrix/vector is time-dependent. The global mass matrix is time-dependent because of the curvature of the vehicle's path. The stiffness matrix, the damping matrix and the loading vector of the whole system all become time-dependent. The EOM's (10) and (11) are numerically integrated in a state-space form with the aid of the available ordinary differential equation solvers for large, stiff systems in MATLAB (MathWorks 1994-2013), verified previously (Dimitrakopoulos & Zeng 2015).

3 RESULTS AND DISCUSSION

Conventional code based seismic response analysis focuses on the performance of solely the bridge structure, under strong earthquake events. On the contrary, the focus of the present paper is on the influence the seismic response of the bridge has on the running vehicles, under moderate (frequent) earthquakes. Therefore, this study compares the following three cases: (i) the dynamic vehicle-bridge-interaction (VBI) analysis, in the absence of earthquakes; (ii) the conventional seismic response analysis of the bridge without vehicle dynamics; and (iii) the seismic response analysis of the interacting vehicle-bridge system (VBI).

The focus of this study is on frequent earthquakes of moderate intensity. As an example, the study considers a historic ground motion recorded on 23 December 1972 in Managua Nicaragua, at Managua ESSO station, for a 5.2 magnitude and an epicenter 4.33 km earthquake event (PEER. 2015). Figure 3 plots the time-histories of the three components of the ground acceleration: upper-down (U-D), north-south (N-S), and east-west (E-W), and the pertinent Fourier Spectra.

The study assumes that before the vehicle enters the bridge, it runs on the rigid embankment and has initial non-zero deformation due to the weight and the lateral (centrifugal and coriolis) forces, when it enters the bridge. The analysis of the VBI starts when the first vehicle enters the bridge and stops when the last vehicle of the train leaves the bridge. After a vehicle leaves the bridge, its response is no longer of interest herein. The speed of the vehicle is 120 km/h (33.33 m/s) and each train consists of ten identical vehicles, with the properties given in Antol ń et al. (2013). The track cant angle is 0.105, according to the design of the railway line. The rails have a knife edge shape and the conicity of the wheels is 0.05. The conventional approach in seismic engineering (e.g. EC8 1998) is to represent the

traffic during an earthquake as an additional quasi-permanent mass. According to EC8 (1998), for railway bridges, the additional mass is: $\psi_{2,1}Q_{k,1}=0.3Q_{k,1}$. The effective flexural stiffness of the piers and the effective torsional stiffness of the deck are taken half the uncracked stiffness (assuming solid sections) (EC8 1998).

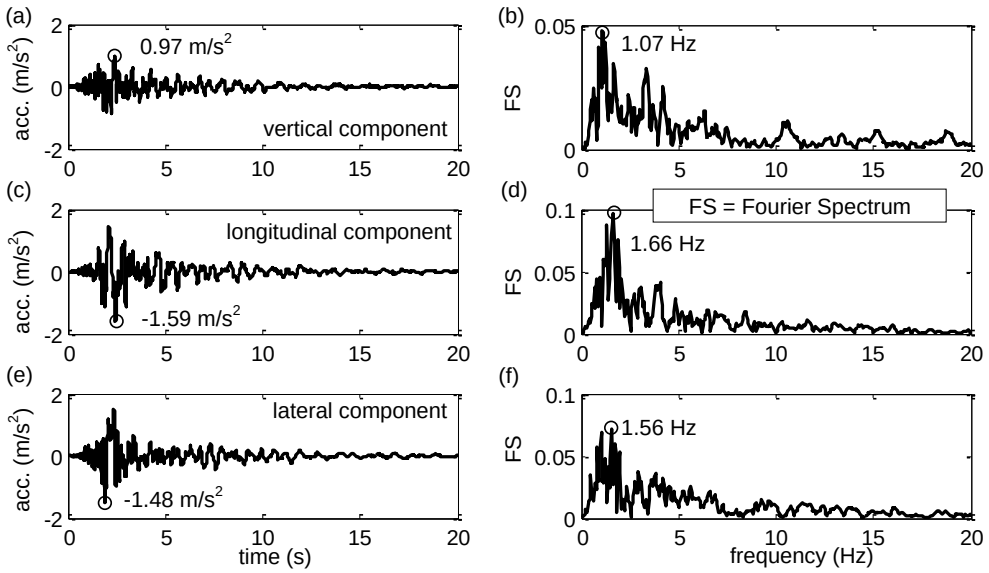

Figure 3. The acceleration time-histories (a, c, e) and the pertinent Fourier Spectra (b, d, f) of the three components of the ground motion recorded in 1972 in Managua Nicaragua, at Managua ESSO station.

The proposed seismic analysis of the VBI system assumes that the earthquake strikes when the first vehicle enters the bridge. Later, different time instants the earthquake occurs are investigated. The mass of the vehicles is modeled directly through the properties of the 3D multibody model with the mass matrix $\mathbf{M}^V$ in Eq. (3), and hence it is unnecessary to increase further the mass by $0.3Q_{k,1}$.

Figure 4 plots the time-histories of the bridge displacement (Figure 4 (a) and (c)) and the pertinent Fourier Spectra (Figure 4 (b) and (d)). The time-histories plots correspond to the three cases (i) to (iii), while the Fourier Spectra to the cases (ii) and (iii). The deformation pattern of the bridge is different, due to the running vehicles (Case 1: blue solid line) and due to the seismic loading (Case 2: gray dotted line), when either is considered independently. Due to the running vehicles (blue solid line) the bridge deflects almost statically downwards in the vertical direction, and in the sense of the centrifugal forces and coriolis forces in the radial direction. On the other hand, the seismic induced bridge vibration is of alternating sign and of higher frequency (gray dotted line). Further, the proposed seismic analysis of the VBI (blue solid line) unveils the combined effects of the dynamic vehicle-bridge interaction (blue solid line) and the seismic shaking (gray dotted line). Under seismic excitation, the deck vibrates about its undeflected (zero) geometry (gray dotted line). However, when the interaction with the vehicles is considered (Case 3: black solid line), the vibration of the deck takes place about the deflected, due to the moving vehicles, geometry. Besides, for the examined ground motion and vehicle model, the earthquake shaking dominates the response of the bridge, rather than the vehicle dynamics. For the pertinent Fourier Spectra (Figure 4 (b) and (d)), the additional mass due to the traffic ($0.3Q_{k,1}$) decreases somewhat the frequencies of the bridge, from 1.57 Hz to 1.48 Hz (Figure 4 (b) and (d)). Recall that the predominant frequency of the lateral component of the earthquake excitation is 1.56 Hz (Figure 3 (f)). It is expected that the radial displacement of the bridge from the proposed seismic analysis is larger than that from the conventional analysis, as 1.57 Hz is closer to 1.56 Hz. However, the result from Figure 4 (c) displays the opposite trend, which is attributed to the damping effect the multibody vehicles on the vibration of the deck. This observation verifies the previous conclusions of Kim et al. (2007).

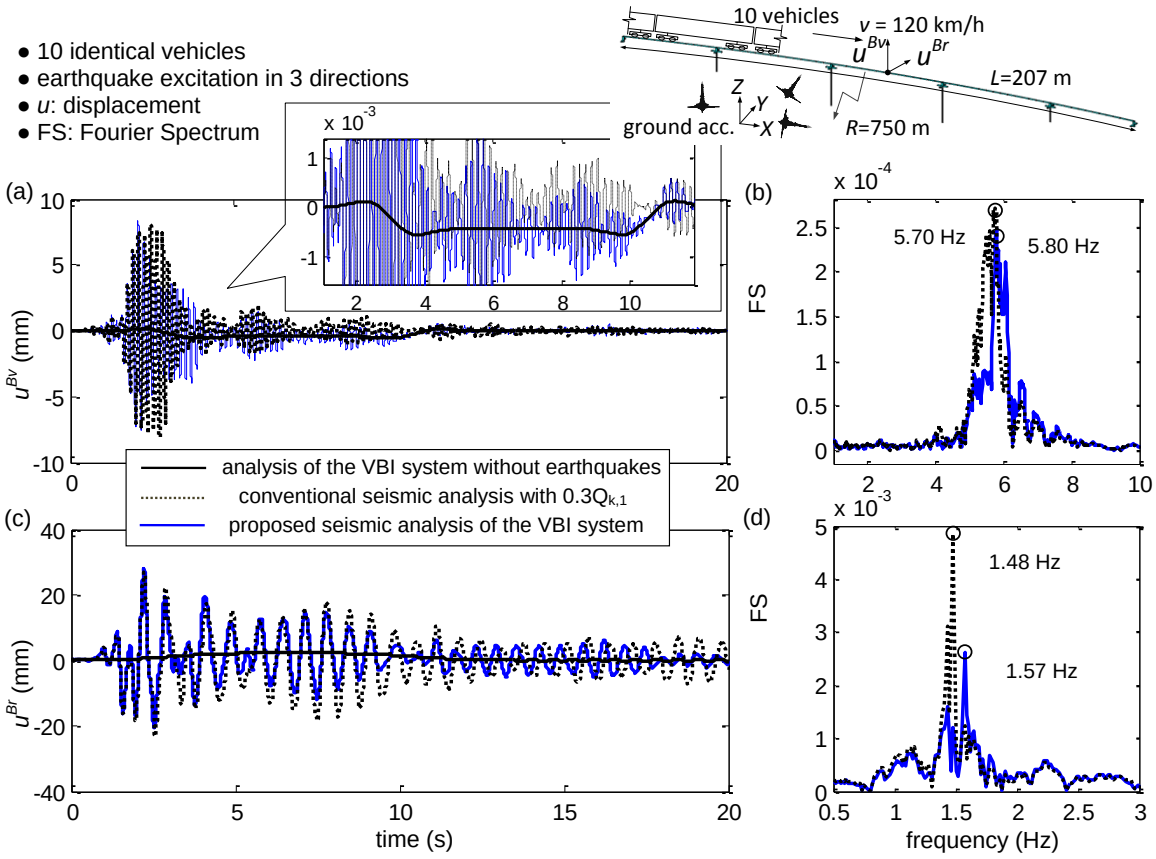

Figure 4. The displacement time-histories of the midpoint of the bridge and pertinent Fourier Spectra: (a and b) the vertical direction and (c and d) the radial direction.

The position of a running vehicle on a bridge when the earthquake strikes, affects the response of the coupled vehicle-bridge system. However, it is unpredictable. Figure 5 investigates the seismic response of the bridge for three different locations of the vehicle on the deck, when the earthquake strikes. These three positions considered correspond to the first vehicle arriving at the midpoint of the first/middle/last span of the deck. The time is set to zero when the first vehicle enters the bridge. Accordingly, the three time instants are 0.54 s, 3.11 s and 5.67 s. Interestingly, the intense part of the seismic response of the bridge shifts in time following the strong ground motion duration of the seismic excitation.

This vehicle-bridge-earthquake 'timing' problem is not so important for the peak response of the bridge. However, it is dominant for the peak response of the vehicle (running on the bridge). Figure 6 investigates the effect of the time instants the earthquake strikes on the response of different vehicles. In particular, Figure 6 shows the accelerations of the car-body which determine the riding comfort, and the derailment factor and the offload factor to assess the operational safety. Recall that, the derail factor is the ratio of the lateral and the vertical contact force acting on the same wheel, whereas the offload factor is the ratio between the dynamic reduction of the vertical contact force (difference between the dynamic and the static contact force) and the static vertical contact force acting on the same wheel. Figure 6 (a) and (b) compares the different time instants the earthquake occurs with distinct line style (as in the legend). The riding comfort of the vehicles exceeds the pertinent contemporary code requirements (Figure 6 (a) to (d)), e.g. (China's Ministry of railway 1986), 2.0 m/s^2 (vertical) and 1.5 m/s^2 (radial), for conventional train vehicles. This result is expected as these code requirements are established for no earthquake conditions. More significantly, the two important metrics of the safety of the running vehicle, the derailment factor and the offload factor, exceed the pertinent thresholds of 0.8 and 0.6, respectively. These results are alarming since they indicate that even frequent earthquakes, of moderate intensity, can threaten the safety of the vehicles running on the bridge during an earthquake.

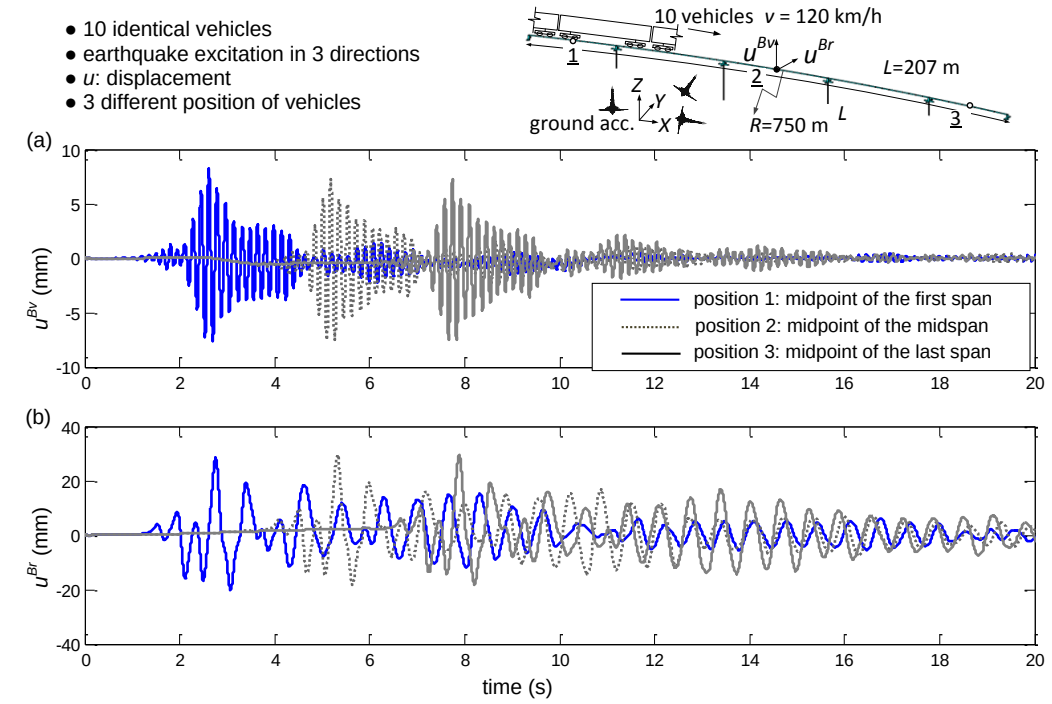

Figure 5. The (a) vertical and (b) radial displacement time-histories of the midpoint of the bridge considering different time instants the earthquake occurs.

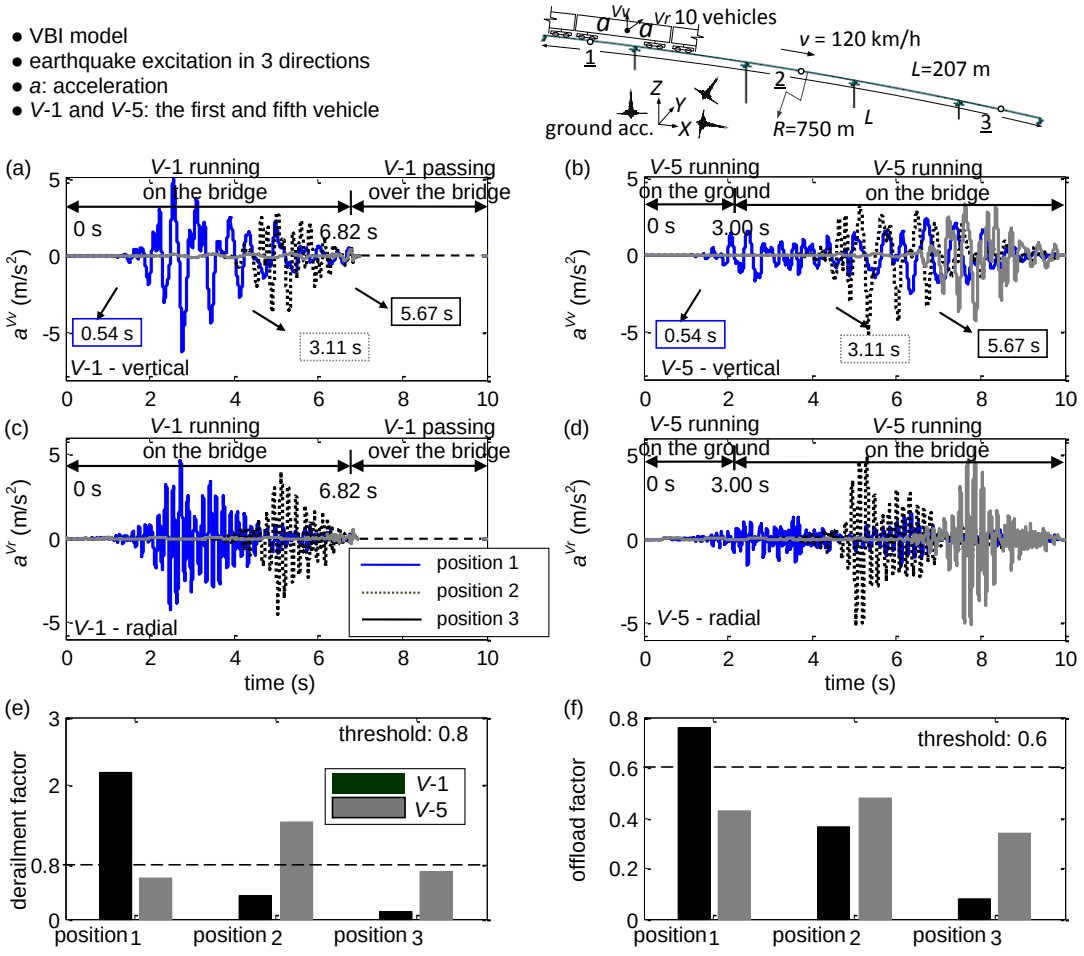

Figure 6. The vertical (a and b) and radial (c and d) acceleration time-histories of the first (a and c) and fifth (b and d) vehicles, and derailment factor and offload factor, considering different time instants the earthquake occurs.

For a vehicle speed of v = 120 km/h and a bridge length L = 207 m, the first and the fifth vehicle are running on the deck from 0 to 6.82 s and from 3.00 to 9.96 s, respectively (Figure 6). The study assumes that each of vehicles and its corresponding DOF's are independent of the adjacent vehicles. The response of the first vehicles is higher when the earthquake strikes earlier (0.54 s), while the response of the fifth vehicle (the latter vehicle) is higher when the earthquake strikes later (3.11 s). As a rule of thumb, the response of the vehicles consistently amplifies, when the strong ground motion shaking finds them running on the bridge, instead of running on the ground.

4 CONCLUSIONS

The present study proposes a scheme for the seismic response analysis of coupled vehicle-bridge systems during (frequent) moderate earthquakes. To demonstrate the proposed methodology, the paper examines a realistic vehicle-bridge interaction case, i.e. a train vehicle model, running at its design speed, during a real earthquake on a realistic railway bridge. The simulation, of both the vehicle and the bridge are three-dimensional. The goal of the work is to study the new problems encountered when analyzing the seismic response of interacting vehicle-bridge systems.

The paper stresses the adverse influence of the earthquake-induced bridge vibration on the riding comfort and the safety of the running vehicles. The results unveil that even frequent earthquakes can threaten the safety of the vehicles running on the bridge during earthquakes. The study verifies the favorable damping effect the running vehicles have on the seismic vibration of the bridge. The particular position of the running vehicles on the deck when the earthquake strikes, affects significantly the response of the vehicle. Clearly, the present study offers only a glimpse into the physics of the complicated and multi-parametric problem, and more research is needed to derive decisive conclusions of general value.

REFERENCES:

ANTOLÍN, P., ZHANG, N., GOICOLEAA, J.M., XIA, H., ASTIZA, M.Á and OLIVAA, J., 2013. Consideration of nonlinear wheel-rail contact forces for dynamic vehicle-bridge interaction in high-speed railways. *Journal of Sound and Vibration*, 332, pp. 1231-1251.

CHINA'S MINISTRY OF RAILWAY, 1986. GB5599-85 Railway vehicles - Specification for evaluation the dynamic performance and accreditation test.

COMITÉ EUROPEEN DE NORMALIZATION, 1998. Eurocode 8: Design of Structures for Earthquake Resistance-Part 2: Bridges. PrEN, 2, pp. 2003.

COOK, R.D., 2007. *Concepts and applications of finite element analysis*. New York: Wiley.

DIMITRAKOPOULOS, E.G. and ZENG, Q., 2015. A three-dimensional dynamic analysis scheme for the interaction between trains and curved railway bridges. *Computers & Structures*, 149, pp. 43-60.

DU, X., XU, Y. and XIA, H., 2012. Dynamic interaction of bridge-train system under non‐uniform seismic ground motion. *Earthquake Engineering & Structural Dynamics*, 41(1), pp. 139-157.

JU, S.H., 2012. Nonlinear analysis of high-speed trains moving on bridges during earthquakes. *Nonlinear Dynamics*, 69(1-2), pp. 173-183.

SHEN, Z.Y., HEDRICK, J.K., ELKINS, J.A., 1983. A comparison of alternative creep force models for rail vehicle dynamic analysis, *Vehicle System Dynamics*, 12 (1-3), pp. 79-83.

KAPPOS A.J., SAIIDI M.S., AYDINOĞLU M.N., ISAKOVIĆ T., 2012. Seismic Design and Assessment of Bridges: Inelastic Methods of Analysis and Case Studies. *Geotechnical, Geological and Earthquake Engineering*, 21.

KIM, C., KAWATANI, M., LEE, C. and NISHIMURA, N., 2007. Seismic response of a monorail bridge incorporating train-bridge interaction. *Structural Engineering and Mechanics*, 26(2), pp. 111-126.

MATHWORKS, 1994-2013. *MATLAB User's Guide*. Natick, MA: The MathWorks Inc.

PEER GROUND MOTION DATABASE PACIFIC EARTHQUAKE ENGINEERING RESEARCH CENTER., 2015-last update. Available: http://ngawest2.berkeley.edu/site [05/04, 2015].

PRIESTLEY, M.N., 1996. *Seismic design and retrofit of bridges*. John Wiley & Sons.

XIA, H., ZHANG, N. and GUO, W., 2012. Application of train-bridge-interaction analysis to bridge design of high-speed railways in China, *Proceedings of the 1st International Workshop on High-Speed and Intercity Railways 2012*, Springer, pp. 355-371.

XIA, H., HAN, Y., ZHANG, N. and GUO, W., 2006. Dynamic analysis of train–bridge system subjected to non-uniform seismic excitations. *Earthquake Engineering & Structural Dynamics*, 35(12), pp. 1563-1579.